A reactive force field simulation of liquid–liquid phase transitions in phosphorus

P. Ballone
Dipartimento di Fisica, Università degli Studi di Messina, Contrada Papardo, I-98166 Messina, Italy and Institut für Festkörperforschung, Forschungszentrum Jülich, D-52425 Jülich, Germany

R. O. Jones[a)]
Institut für Festkörperforschung, Forschungszentrum Jülich, D-52425 Jülich, Germany

(Received 23 July 2004; accepted 6 August 2004)

A force field model of phosphorus has been developed based on density functional (DF) computations and experimental results, covering low energy forms of local tetrahedral symmetry and more compact (simple cubic) structures that arise with increasing pressure. Rules tailored to DF data for the addition, deletion, and exchange of covalent bonds allow the system to adapt the bonding configuration to the thermodynamic state. Monte Carlo simulations in the N-P-T ensemble show that the molecular (P_4) liquid phase, stable at low pressure P and relatively low temperature T, transforms to a polymeric (gel) state on increasing either P or T. These phase changes are observed in recent experiments at similar thermodynamic conditions, as shown by the close agreement of computed and measured structure factors in the molecular and polymer phases. The polymeric phase obtained by increasing pressure has a dominant simple cubic character, while the polymer obtained by raising T at moderate pressure is tetrahedral. Comparison with DF results suggests that the latter is a semiconductor, while the cubic form is metallic. The simulations show that the T-induced polymerization is due to the entropy of the configuration of covalent bonds, as in the polymerization transition in sulfur. The transition observed with increasing P is the continuation at high T of the black P to arsenic (A17) structure observed in the solid state, and also corresponds to a semiconductor to metal transition.
[DOI: 10.1063/1.1801271]

I. INTRODUCTION

Recent x-ray diffraction measurements[1] have identified a liquid-liquid phase transition in phosphorus occurring at high pressure P and temperature T (1 GPa, 1050 C) and interpreted it as a transition from molecular (low P) to polymer (high P) systems. The transformation occurs reversibly over a very small (0.02 GPa) range of P and is detected by a sudden change in the structure factor. The change in the diffraction patterns recorded during a slow pressure scan suggests that the phases transform directly into each other and coexist during the transformation, indicating a first-order transition. Other measurements[2] have determined the transition line over an extended range of P (0.3–1 GPa). Decreasing P enhances the stability of the molecular phase, and the transition temperature increases to 2200 K at 0.3 GPa. These results have renewed interest in the phase diagram of phosphorus, whose complexity has provided surprises and challenges for decades.[3,4]

Part of the P-T phase diagram of phosphorus is shown in Fig. 1. The commonest (white) form at low T and P is a highly reactive wax comprising P_4 tetrahedra, and the most stable form is orthorhombic black P, which has a regular stacking of bilayers. Each atom has covalent bonds with two neighbors in the same layer, and a third in the conjugated layer.[5] The amorphous red form of P is a network of threefold coordinated atoms and is far less reactive than white P, but less stable than black P. *All* forms melt at low P (and different T_m) to give a liquid comprising P_4 tetrahedra.[6] At low T and for $P>4.5$ GPa, the layered structure of black P transforms to a three-dimensional (3D) geometry related to the arsenic (A7) structure[7] and often viewed as a Peierls distortion of a simple cubic (sc) lattice. This first-order phase transition is accompanied by a semiconducting to metal transition,[8] and the transition pressure decreases rapidly with increasing T, reaching 3 GPa near the melting temperature of black P. Other crystalline polymorphs and several amorphous or vitreous forms are stable or metastable under different conditions of P and T, or are formed reproducibly by heating.[9]

Polymerization in P with increasing pressure and T was predicted by simulations[10] based on density functional methods (DF-MD), and recent DF-MD simulations investigated the mechanisms of the transition inaccessible to experiments.[11,12] The results are consistent with the liquid-liquid phase transition described above, but the simulations considered small samples (64 and 100 atoms, respectively) and times of the order of picoseconds. The transition shows analogies to polymerization in sulfur at T_λ (432 K at 1 atm), and has another similarity between P and S. Each has many polymorphs,[3] and all melt to the same low viscosity molecular liquid: P_4 tetrahedra and S_8 rings, respectively. P and S

a)Electronic mail: r.jones@fz-juelich.de

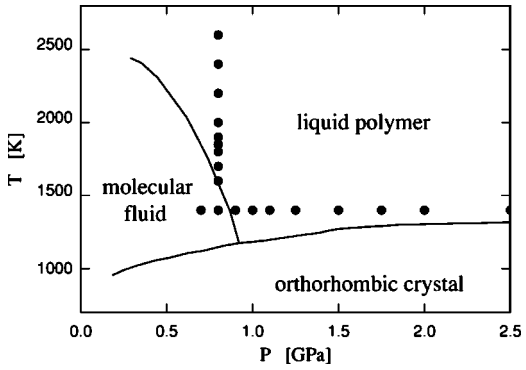

FIG. 1. Schematic phase diagram of phosphorus. The points represent (P,T) coordinates of the present simulations.

are semiconductors under normal conditions, but become metallic at P well within the reach of current experimental methods.[13,14]

Our recent computer simulation of polymerization in S was based on a realistic interatomic potential[15,16] and showed that the transition is driven by the entropy associated to the distribution of covalent bonds, i.e., a sulfur sample can be viewed as an assembly of N atoms and M $(M \leqslant N)$ bonds. The low T molecular phase comprising mainly S_8 units[17] is one such configuration. The accessible phase space increases with increasing T, as bonds break, form, and rearrange among atom pairs. Most bond configurations are long S_n chains in a polymeric phase. The entropy of the chains competes with translational entropy, which favors small molecular species, and the balance determines the transition point.

Similar effects should lead in P to a line between a liquid comprising P_4 molecules and a polymeric liquid. Obvious differences between P and S are their valences and the different roles of potential energy, which favors the connected phase in P and the molecular phase in S. The observation of a liquid-liquid transition in P then provides a second system to study using the strategy, model, and methods used in sulfur, as well as allowing us to investigate the effects on the transition of different bonding and thermodynamic properties.

We have investigated this transition by simulations based on a reactive force field (FF) incorporating experimental data for the P-T phase diagram and information provided by DF computations for the geometry, energy, and reactivity of small phosphorus aggregates. The DF results show that P_4 tetrahedra can be deformed to a roof structure with radicals at two extremities. This reaction requires a significant energy, but the activated species enters a propagation reaction—analogous to S polymerization—that leads to the growth of phosphorus aggregates.[18,10] Other mechanisms are possible, since P has more bonding motifs even at moderate (P,T). Our main aim is to extend the length and time scales well beyond those accessible to DF-MD, with particular focus on the thermodynamic properties and the driving force behind polymerization. The force field also allows us to characterize the potential energy surface in terms of a few energy and length parameters, providing a link between bonding properties and the polymerization transition. Units of energy and length are kcal/mol and Å, respectively. A preliminary account of the work has been given in Ref. 19.

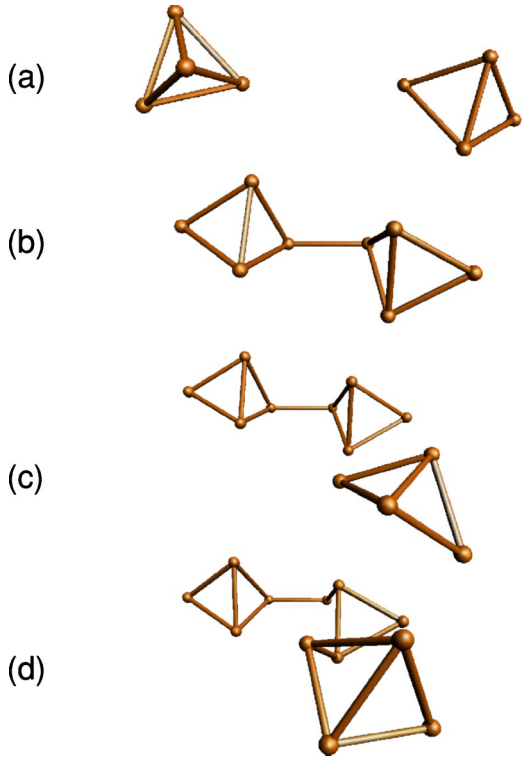

FIG. 2. Reactions studied by all-electron DF calculations: (a-b) Triplet C_{2v} radical reacts with P_4-tetramer, (c-d) resulting P_8 molecule reacts with additional triplet radical.

II. DENSITY FUNCTIONAL COMPUTATIONS

Experimental information on such polymers is scarce and often indirect, so that DF calculations of the energies and geometries for small P_n clusters provide essential input for the development of the FF. DF studies of P_n up to $n=11$ (Refs. 20 and 21) highlight their tendency to form tubular structures, but these are unlikely in simulations where kinetic constraints and free energy are more important than potential energy. However, the near degeneracy of P_8 with $2P_4$, and the slow convergence of the cohesive energy per atom to the bulk limit imply that entropy plays an important role for the cluster growth even at very small sizes.

All-electron DF calculations[22] have been used to investigate activated clusters and reaction mechanisms. Examples of the results are shown in Fig. 2: (a) A P_4 tetrahedron opens to a triplet radical C_{2v} roof structure [right] and reacts with another tetrahedron to give the radical (b). The reaction with another triplet (c) then leads to the chain structure (d). The DF results show that opening a P_4 tetrahedron to the triplet radical requires over 1.9 eV, but the reaction (a-b) has a very small energy barrier ($\sim$0.1 eV), and (c-d) is barrierless. These results are consistent with the observation of linear structures in DF simulations,[10] and explain the presence of similar structures in the early stages of polymerization during the present simulations.

The configuration changes shown in Fig. 2 can be viewed as bond interchanges combining bond breaking and

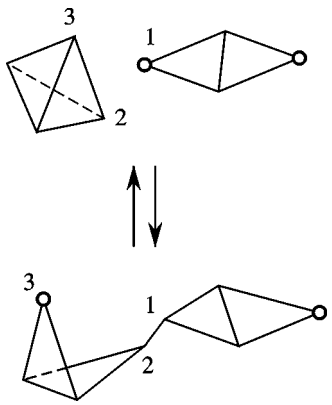

FIG. 3. Bond interchange mechanism at divalent radical terminations (identified by circles).

formation for triplets of neighboring atoms. In our model they always involve one twofold coordinated atom and take place according to the mechanism in Fig. 3.

III. THE INTERATOMIC POTENTIAL

A. Development of the interatomic potential

The complex chemical behavior of P requires a more detailed model than commonly used, and we use a FF that reproduces the energetic and structural properties of P_4, small P_n aggregates, and black P. Additional features (coordination changes, dependence of force constants on coordination) and free parameters are added to describe the phase transitions discussed above. Each additional degree of freedom affects mainly one structural, kinetic or thermodynamic property, thus simplifying the tuning of the potential and the interpretation of the results.

In traditional FF models, the system is an assembly of atoms and covalent bonds. Here, bonds are not defined simply in terms of interatomic distances, but by binary variables (the bond is either on or off) associated to atom pairs. Each atom can form from two to six bonds, which determine the intramolecular and intermolecular contributions to the potential energy. *Undercoordinated* atoms (coordination number $n_c=2$) are reactive radicals, *regular* atoms are threefold coordinated (standard at moderate P and T), and those with higher coordination ($4\leqslant n_c\leqslant 6$) are *overcoordinated*, such as those found in high P polymorphs. Experiments and DF computations show that, with increasing coordination, phosphorus undergoes a sequence of transitions from semiconductor (black P, A17 structure) to semimetal (A7 structure) and to metal (sc, bcc, and simple hexagonal).[23,24]

Breaking the bond between atoms i and j involves an energy change $\Delta E_b=\delta E_i^b+\delta E_j^b$, which is the sum of n_c-dependent contributions from the atoms: $\delta E_i=+16.5$, $+2,+2$, and -10 kcal/mol for $i=3$, 4, 5, and 6, respectively. These values are based on DF results and computational considerations, e.g., δE_3^b is a compromise between the DF value (22 kcal/mol), and the need to have sufficient twofold coordinated atoms to enhance relaxation. The values for $i\geqslant 4$ reflect the low stability of overcoordinated atoms at low P and T. Similarly, bond formation involves an energy $\Delta E_f=\delta E_i^f+\delta E_j^f$ with $\delta E_i^f=-16.5,-2,-2$, and $+10$ kcal/mol for $i=2,3,4$, and 5, respectively.

TABLE I. Parameters of the intramolecular potential energy (energies in kcal/mol, distances in Å, angles in degrees.

K_s ($n_c\leqslant 3$)	K_s ($n_c\geqslant 4$)	d_0	K_b	K_b'	θ_0	θ_1	S_b	K_τ
297	208	2.19	26.7	53.4	109	60	0.2	0.064

The intramolecular energy U_b is the sum of stretching, bending, and torsion contributions:

$$U_b[\mathbf{R}_1,\ldots,\mathbf{R}_N]=\frac{1}{2}\sum_{\langle ij\rangle}K_S^{\langle ij\rangle}(d_{ij}-d^0)^2+\sum_{\langle ijk\rangle}F^j(\cos\theta_{ijk})+\sum_{\langle ijkl\rangle}G[\tau_{ijkl}]. \tag{1}$$

Here $d_{ij}=|\mathbf{R}_i-\mathbf{R}_j|$, and θ and τ are bending and torsion angles, respectively, identified by three ($\langle ijk\rangle$) and four ($\langle ijkl\rangle$) atoms connected by consecutive covalent bonds. Each distance, bending and torsion angle is counted only once in the sums, and d^0 is the equilibrium bond length in P_4 (2.19 Å). The stretching and bending terms depend on the coordination of the atoms involved, in order to mimic the changes of stretching and bending force constants,[25] and the change of local symmetry (tetrahedral to sc). The stretching force constant $K_S^{\langle ij\rangle}$ for bonds joining regular atoms is obtained by fitting the A_1 vibrational frequency of P_4.[26] $K_S^{\langle ij\rangle}$ is reduced by 30% if at least one atom is overcoordinated, thus reducing the stretching frequency by 15%. The role of the bending potential is more important and more subtle. The functional form of $F^j(\cos\theta_{ijk})$ depends on the coordination of the pivot atom j in the $\langle ijk\rangle$ triplet. If atom j is undercoordinated or regular ($n_c(j)=2,3$), F^j is a fourth-order polynomial,

$$F^j(\theta_{ijk})=\tfrac{1}{2}K_b(\cos\theta_{ijk}-\cos\theta_0)^2\times[(\cos\theta_{ijk}-\cos\theta_1)^2+S_b]. \tag{2}$$

If j is overcoordinated $[n_c(j)=4,5,6]$, F is a piecewise polynomial:

$$F^j(\theta_{ijk})=K_b\cos^2\theta_{ijk}(\cos\theta_{ijk}-\cos\pi)^2\times[(\cos\theta_{ijk}-\cos\theta_1)^2+S_b],\quad \cos\theta_{ijk}<0 \tag{3}$$

and

$$F^j(\theta_{ijk})=\tfrac{1}{2}K_b\cos^2\theta_{ijk},\quad \cos\theta_{ijk}\geqslant 0. \tag{4}$$

K_b, S_b, θ_0, and θ_1 are listed in Table I, and $F^j(\theta_{ijk})$ is shown in Fig. 4 for regular and overcoordinated atoms. In regular atoms, $F^j(\theta_{ijk})$ has a minimum at the tetrahedral angle $\theta_0=109°$ and shows a marked softening at $\theta_1=60°$, the bond angle of the P_4 tetrahedron. For overcoordinated atoms, minima at $\theta=90°$ and 180° favor a sc geometry.

The torsional contribution

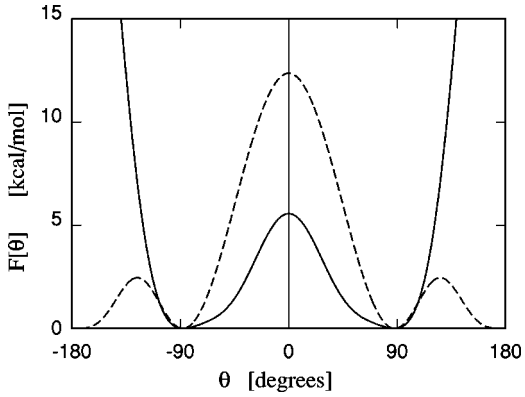

FIG. 4. Angle and coordination dependence of the bending energy. Full line: $F^j(\theta_{ijk})$ for regular j atoms ($n_c=2,3$); dash line: overcoordinated j atoms ($n_c \geqslant 4$).

$$G[\tau] = \tfrac{1}{2} K_\tau \cos^2 \tau (\cos^2 \tau - 1)^2 \tag{5}$$

does not depend on the coordination of the atoms involved, and the minima at $\tau = 0$, $\pi/2$, and π reproduce the relative stability of small P clusters. The force constants K_b and K_τ are determined by fitting the frequencies of the E and F_2 modes of P_4.

The intermolecular energy U_{nb} is given by a Lennard-Jones (LJ) potential

$$U_{nb} = 4\epsilon \sum_{i<j}^{N'} \left[\left(\frac{\sigma_{ij}}{r_{ij}} \right)^{12} - \left(\frac{\sigma_{ij}}{r_{ij}} \right)^{6} \right] \tag{6}$$

up to $r = 3\sigma$.[27] The prime indicates that pairs of atoms joined by a covalent bond are excluded from the sum. A modification of the interaction between pairs joined by two consecutive bonds is required to avoid a short range repulsion that would prevent the growth of aggregates beyond P_4 (for which all atoms are first neighbors). It is obtained by an 8% reduction of the corresponding σ.

The indices on σ_{ij} indicate its dependence on the coordination of the atoms involved, and the (ϵ,σ) parameters for pairs of threefold coordinated atoms ($\epsilon = 0.4$ kcal/mol, $\sigma_{33} = 3.33$ Å) have been determined by fitting the experimental volume and cohesive energy of white P. The same ϵ is used in all cases, and $\sigma_{ij} = 3.33$ Å for all pairs that do not involve undercoordinated atoms. The LJ diameter is reduced to 2 Å if at least one of the two atoms is undercoordinated, reflecting the findings of Sec. II and allowing the model to mimic the high reactivity of undercoordinated P atoms. In our simulations, the small size of undercoordinated atoms results in (i) the stabilization of a small population (a few percent) of twofold coordinated atoms at P exceeding 1 GPa, (ii) a reduced energy barrier for the interchange of covalent bonds, and thus in (iii) an enhanced sampling of bond configurations.

B. The simulation method

Monte Carlo (MC) computations have been performed in the N-P-T ensemble. The simulation consists of single particle moves, whole molecule translations, and volume changes. Single particle moves are attempted most often and provide a natural clock for our simulations. Whole molecule translations are attempted, on average, every 20 single particle moves and contribute greatly to the average atomic displacement in the molecular phase. However, their acceptance probability decreases rapidly on polymerization. A cubic simulation cell is adopted for the constant P simulation of liquid samples, and volume changes are restricted to the isotropic rescaling of coordinates. Volume changes are attempted, on average, every 1.25 single atom moves *per atom*. Additional moves have been introduced to sample different configurations for the covalent bonds. The major difficulties they pose concern the enforcement of microscopic reversibility, and the low acceptance ratio, resulting in long relaxation times.

The bond configuration can change by single bond breaking and formation. An atom is selected at random for each bond breaking attempt, and the move is rejected if this atom has only two covalent bonds (every atom is at least twofold coordinated). Otherwise, a second atom is selected randomly within a sphere of radius $R_b = 5$ Å centered on the first. Bond breaking is attempted if the two atoms form a covalent bond, and accepted or rejected with probability given by the Boltzmann factor for the energy change (which includes bonded and nonbonded contributions and the bond energy ΔE_b). An equivalent strategy is used for bond formation: An atom is chosen randomly and, if sixfold coordinated, the move is rejected. Otherwise, a second atom is selected at random within a sphere of radius R_b centered on the first. If this second atom also has fewer than the maximum number of bonds, a covalent bond is formed between the first and second atom. This change is followed by an acceptance-rejection decision based on the Metropolis rules.

Bond breaking and formation should suffice to establish equilibrium with respect to the bonding configuration, but the process is exceedingly slow for realistic choices of ΔE_b and ΔE_f. Relaxation has been enhanced by adding bond-interchange moves using the mechanism shown in Fig. 3. The entire process (bond breaking and formation) conserves the number of bonds, and often involves an energy barrier lower than in individual bond breaking or formation.

Care is required here to ensure microscopic reversibility. The bond interchange is attempted by selecting a random atom. If this is twofold coordinated, a second atom is selected randomly within a distance R_b from the first, and the move is rejected if the second atom is also undercoordinated. Otherwise, bond interchange is attempted (Fig. 3), and acceptance/rejection is decided according to standard MC rules. The acceptance rate of this process is usually limited by the low concentration of twofold coordinated atoms and enhanced by increasing P. This reduces the asymmetry between bonded and nonbonded interatomic distances and reduces the energy cost of interchanging bonds. One of the bond changing moves, i.e., breaking, forming, and interchange, is selected at random with equal probability, and attempted following each single particle move.

Convergence of the bond configuration is monitored by (i) the rate of accepted moves changing the bond configurations, (ii) the stabilization of density and average potential energy, and (iii) the dynamical equilibrium of different mo-

lecular sizes. For the thermodynamic conditions of our simulations, equilibration is achieved after 10^6 single particle moves per atom. An equal number of steps has been used to accumulate statistics after equilibration under the same conditions.

C. Test of the interatomic potential

The model is designed to study the polymerization transition observed at high T/high P, since the description of the full phase diagram (including the low T/low P polymorphs) is far beyond any empirical model of acceptable complexity.[28] It should nevertheless describe as many features as possible while avoiding unphysical phases, and this may occasionally require sacrificing quantitative accuracy in favor of global reliability. In P_4, for example, the model reproduces exactly the tetrahedral geometry with a bond distance of 2.19 Å, but vibrational frequencies [$\nu_2(E) = 340\ \mathrm{cm}^{-1}$, $\nu_3(F_2) = 478\ \mathrm{cm}^{-1}$, $\nu_1(A_1) = 670\ \mathrm{cm}^{-1}$] differ from measured values (362, 459, and 600 cm^{-1}, respectively, measured at 12 K in a crystal P_4 phase).[26] We have shown that an unconstrained fit can reproduce the experimental vibrational frequencies of P_4 (at a given reference temperature), and the deviations between computed and measured frequencies are the penalty for being able to reproduce better the energy ordering of clusters and connected phases.

For clusters larger than P_4, the reference geometries and energies are provided by DF calculations.[20,21] The energy of an isolated atom is not defined by the model, so that absolute cohesive energies are not accessible. However, the model provides the energies of all aggregates with three or more atoms (i.e., those where all atoms are at least twofold coordinated), and relative cohesive energies can be compared for all P_n with $n \geqslant 3$. The most stable P_8 isomer C_{2v} differs in energy from $2P_4$ by less than 0.02 eV/atom in the generalized gradient approximation (GGA), and two other P_8 isomers, including the cube, are within 0.18 eV/atom of the C_{2v} form.[29] The geometries of the three isomers are reproduced fairly well, and the cohesive energies differ by less than 0.12 eV/atom. The energy ordering is not correct, since the P_8 cube is the most stable, almost degenerate with the C_{2v} form.[20] We emphasize, however, that the model reproduces the near degeneracy of P_8 and $2P_4$, which affects growth trends and pathways. The cohesive energies predicted by the model for P_n up to $n=11$ atoms differ from the DF-GGA results by only ~ 0.05 eV/atom, which is similar to the cohesive energy differences obtained with different DF schemes.

The properties of white P have been used to fit the LJ parameters and are reproduced by the model. Furthermore, orthorhombic black P is locally stable and displays no tendency to deform significantly during long simulations at low P and T [up to (0.5 GPa, 600 K)]. Black P is 5.6 kcal/atom more stable than white P, and its equilibrium density ($2.8\ \mathrm{g/cm}^{-1}$) agrees well with the experimental value ($2.7\ \mathrm{g/cm}^{-1}$).

The extension of the potential to cover coordination to $n_c=6$ allows a variety of crystal structures far greater than possible with $n_c=3$. We focus on coordinations four and six since no structure with coordination five seems to be relevant. The regular stacking of square 2D lattices with in-plane covalent bonding is only 1 kcal/atom less stable than black P. This form might be related to a layered phase, but its relatively low energy may be an artifact of our choice of potential parameters. However, no phase with this motif appeared during simulations, and its presence does not affect the results.

At zero pressure cubic P is 2.5 kcal/atom less stable than black P, but it has a higher density ($4.5\ \mathrm{g/cm}^3$ for the model, $3.85\ \mathrm{g/cm}^3$ measured) and is stabilized as P increases. The enthalpy per atom $h=u+Pv$ (where u and v are the potential energy and the volume per atom, respectively) of the cubic phase becomes lower than that of black P at 2.7 GPa, thus underestimating the experimental stability boundary (3-4.5 GPa).[30] The overestimate of the sc density and the related underestimate of the black P to sc transition pressure are due to the assumption that the P-P covalent bond length is independent of coordination. Experimental data, instead, show that this length increases by $\sim 6\%$ in going from black to cubic P. This effect could be easily included in further refinements of the model.

IV. SIMULATION RESULTS

Liquid samples comprising 1000 P_4 tetrahedra, equilibrated at (0.5 GPa, 1400 K) at fixed bonding ($n_c=3$ for each atom), have been compressed or heated while switching on the bond dynamics. As shown in Fig. 1, ten simulations have been performed at $T=1400$ K ($P=0.7$, 0.8, 0.9, 1, 1.1, 1.25, 1.5, 1.75, 2, and 2.5 GPa), and a further ten at $P=0.8$ GPa ($T=1400$, 1600, 1700, 1800, 1850, 1900, 2000, 2200, 2400, and 2600 K). Both sequences bracket transformations from a molecular liquid to a polymer.

Switching on the bond dynamics results in all samples in a small population of undercoordinated atoms and more bond interchanges. At (0.7 GPa, 1400 K) the relaxation of the bond distribution leads to a significant population of species larger than P_4. However, the growth of molecules is limited to a relatively narrow size range, with 92% of the total mass involving molecules with $n \leqslant 20$, while P_4 alone still accounts for more than 50% of all atoms. These observations are quantified by the size probability distribution, which decreases rapidly and monotonically with increasing n starting from its maximum at $n=4$. Our simulation rules prevent the formation of P_n species smaller than P_4.[31] The equilibrium density at (0.7 GPa, 1400 K) is $1.75\ \mathrm{g/cm}^3$, and the concentration of different coordinations is 2.0%, 93.9%, 3.8%, 0.3%, and 0% for $n_c=2$, 3, 4, 5, and 6, respectively. The structure factor agrees well with the experimental data measured under similar (P,T) conditions. Figure 5 shows that $S(K)$ displays a narrow and high peak at $k = 1.35\ \mathrm{Å}^{-1}$, and a broader peak between 2.5 and $4\ \mathrm{Å}^{-1}$. The asymmetry of this second peak indicates a superposition of two contributions (at 2.8 and $3.5\ \mathrm{Å}^{-1}$), with the latter having more weight. In Ref. 12 the first $S(K)$ peak at $k = 1.35\ \mathrm{Å}^{-1}$ is attributed to the correlation among the centers of mass of P_4 molecules. This peak is a reliable indicator of the stability of local tetrahedral bonding but is not related

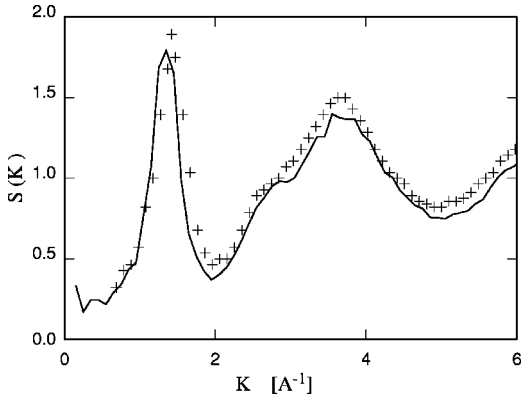

FIG. 5. Comparison of computed (full line, $T=1400$ K, $P=0.7$ GPa) and experimental (crosses, $T=1313$ K, $P=0.77$ GPa) structure factor. Experimental data are from Ref. 1.

directly to the stability of individual P_4 units. We describe the transition induced by compression, and then the T-induced polymerization process.

The density increases monotonically on increasing P at constant T (1400 K) and the bonding pattern changes. The latter are the most apparent effects of compression. The size $N_{\max}$ of the largest aggregate found in each sample at the end of the equilibration stage, for instance, shows a dramatic rise in compressing from $P=1$ GPa to 1.1 GPa (Fig. 6), pointing to a phase transition taking place at $P_{polym}=1.1$ and complete at 1.25 GPa. The size of the largest cluster in a single configuration is not a reliable indicator of the state, since this quantity fluctuates significantly during the simulation, but integrated and average quantities provide an equivalent picture. Because of finite size effects, the estimate of the transition pressure depends on the quantity used to monitor the system. The average size $N_{aver}^{(>20)}$ of aggregates larger than 20 atoms, for instance, displays the largest variations for P slightly higher than P_{polym} estimated from $N_{\max}$, because in the vicinity of the polymerization line large aggregates coexist with several medium-size molecules. The quantities $N_{\max}$ and $N_{aver}^{(>20)}$ nearly coincide at high P (Fig. 6), since in most configurations almost all atoms form a single large aggregate.

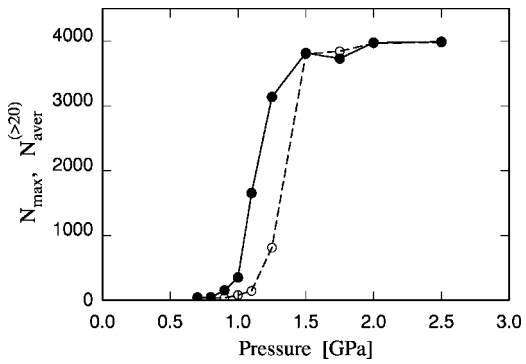

FIG. 6. Size $N_{\max}$ of the largest cluster at the end of the equilibration stage as a function of P at $T=1400$ K (solid dots and full line); Average size $N_{aver}^{(>20)}$ of aggregates larger than 20 atoms (empty circles and dash line). The simulated system consists of 4000 atoms.

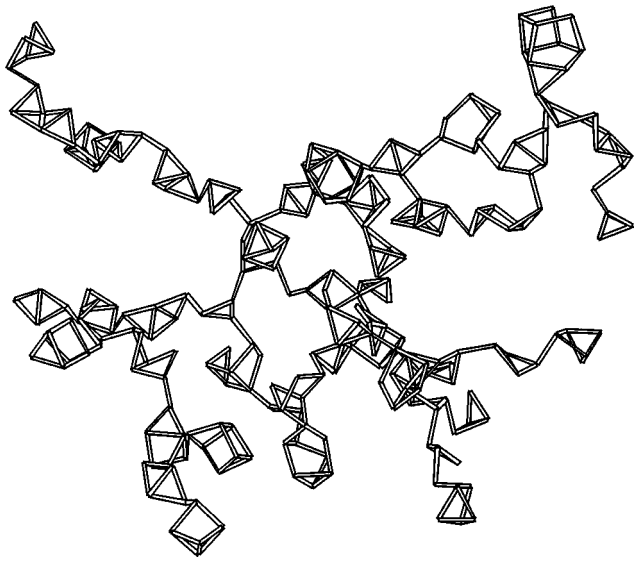

FIG. 7. Phosphorus clusters in the nucleation stage of the molecular to polymer transition.

In the early stages of P-induced polymerization it is possible to find linear chains of P_4 rhombuses (Fig. 7), reminiscent of the structures predicted by Pauling and Simonetta.[18] However, branching grows in importance as equilibrium is approached. A critical assessment of the Pauling-Simonetta model[32] (see also Ref. 10) noted that linear chains of P_4 units joined by single bonds are less stable than their P_4 constituents and unlikely precursors of polymerization. Our results show that entropy does not substantially stabilize chainlike structures, although kinetic factors make them relevant in the initial stages of polymerization. Because of branching and 3D-connectivity, the polymeric phase should be referred to as a gel.

Polymerization is reflected in changes of $S(K)$ very similar to those measured (Fig. 8). Increasing P on the low density molecular phase at (0.7 GPa, 1400 K) results in a monotonic but slow reduction of the $S(K)$ peak at 1.35 Å^{-1} $[S(K_1)]$, which remains the dominant feature in $S(K)$ up to 1.1 GPa. In the same range, P-induced changes in the broad peak at $2.5 \leqslant K \leqslant 4$ Å^{-1} are limited to a slight increase in the weight of the 2.8 Å^{-1} contribution at the expense of the 3.5 Å^{-1} one. Significant changes are observed on increasing P from 1.1 to 1.25 GPa, for which the $S(K_1)$ peak is visible but not dominant, while a double peak structure develops in the $2.5 \leqslant K \leqslant 4$ range. Above 1.25 GPa, the P dependence of $S(K)$ is again weak, being mainly a further reduction of the $S(K_1)$ peak, which practically disappears for $P \geqslant 2$ GPa. It is not obvious whether the residual weight in the $S(K_1)$ peak at 1.25 GPa is an equilibrium feature or an artifact of slow relaxation in the proximity of the transition point. There are clear similarities between experimental and computational results (Fig. 8), despite differences in the transition pressure (1 GPa in the experiment, and between 1.1 and 1.25 GPa in our simulations). We note that differences between the measurements of two groups[1,2] at similar thermodynamic conditions are almost as large as the discrepancies between simulation and each of the experimental $S(K)$'s. Moreover, tests

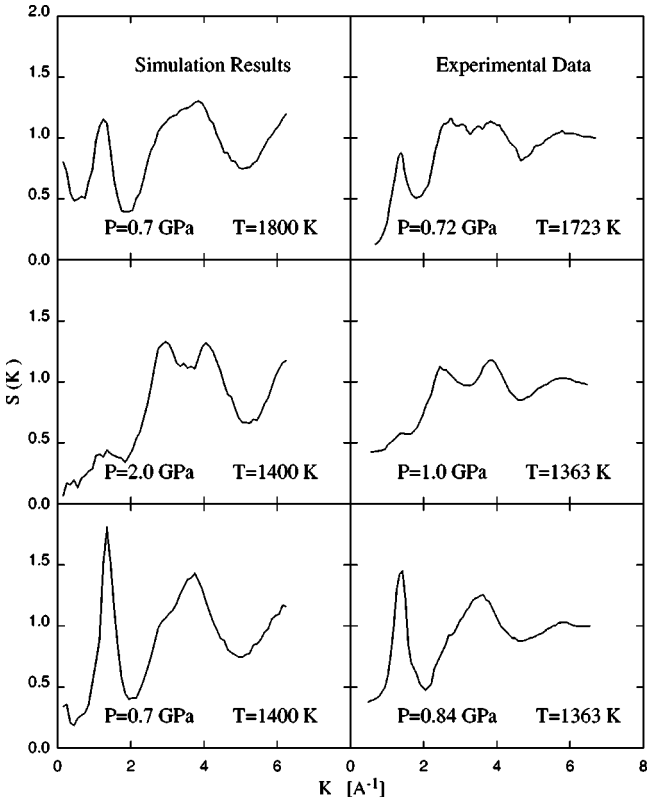

FIG. 8. Calculated and measured (after Ref. 2) structure factors for different P and T. The simulation result for (2 GPa, 1400 K) has been shifted by 0.5 units along the y direction.

showed that the quantitative inaccuracies in $S(K)$ are reduced greatly by assuming that the covalent bond length d^0 depends weakly on bonding, going from $d^0=2.19$ Å for threefold coordinated atoms to $d^0\sim 2.28$ Å, as suggested by the experimental data on $S(K)$. All our results assume $d^0=2.19$ Å.

The changes in the real-space correlations due to polymerization are summarized by the plot of the radial distribution functions in Fig. 9. The peak at $r=2.20$ Å is the dominant feature of $g(r)$ at all thermodynamic conditions considered in the present study, and even its precise location does not depend significantly on P and T. In simple liquids, the first peak of $g(r)$ is followed by a regular sequence of

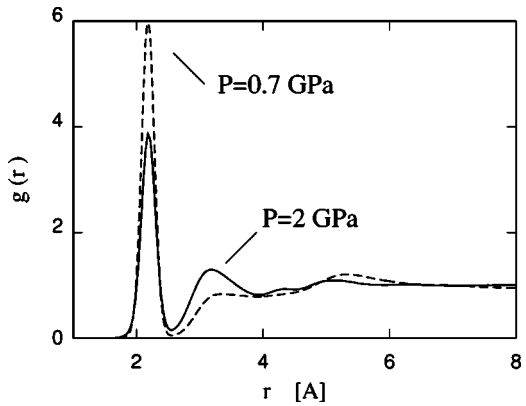

FIG. 9. Pressure dependence of the radial distribution function across the polymerization transition.

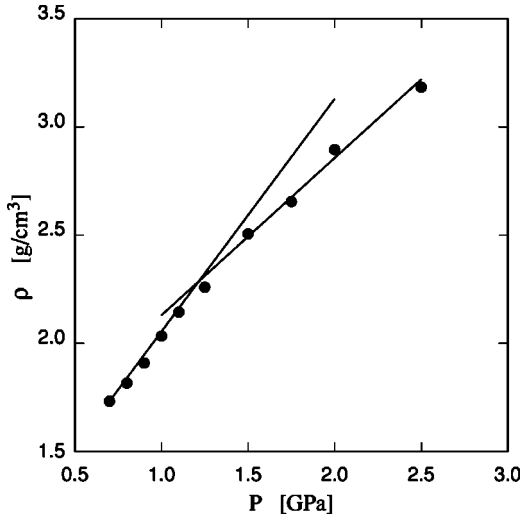

FIG. 10. Pressure dependence of the average density at $T=1400$ K.

secondary peaks, whose amplitude decreases with increasing distance from the origin. In molecular fluids, instead, the high and narrow peaks due to covalent bonds are often followed by complex patterns of next-neighbor correlations, revealed by low amplitude oscillations in $g(r)$ that extend up to fairly long distances ($\sim$15 Å). The radial distribution function computed at low P and T displays the characteristic features seen in molecular liquids that arise from the competition of covalent and nonbonded packing distances. The most obvious change in $g(r)$ upon polymerization is the appearance of a peak at 3.15 Å, due to atom pairs that are second neighbors along the bond network, i.e., pairs that are not covalently bonded, but linked to a common atom by nearly orthogonal bonds. The large increase in the concentration of these pairs requires the growth of connected aggregates, since in the original P_4 fluid all atoms belonging to the same covalent unit are first neighbors. It also requires a change in the local geometry, increasing coordination and favoring sc over tetrahedral structures. We (i) emphasize that both structural transformations must take place simultaneously to observe the changes shown in Fig. 9, that, in turn, are reflected in the $S(k)$ evolution reproducing the experimental trends; and (ii) show below that polymerization can take place (with increasing T) even without the transformation in the local coordination, leaving $g(r)$ almost unchanged.

The density ρ depends linearly on P with different slopes below and above polymerization (Fig. 10), and the compressibility is significantly lower in the polymer phase. The results for $\rho(P)$ suggest that polymerization here is a continuous transition, possibly marked by discontinuous variations of the response functions [the isothermal compressibility for $\rho(P)$]. However, a weakly first-order transition cannot be excluded, since finite size effects are important for samples of 4000 atoms and might mask a slight discontinuity in the density.

We have noted that the changes in structural and thermodynamic properties with increasing P are accompanied by a change in the dominant local coordination. Threefold coordinated atoms are the only relevant species at (0.7 GPa, 1400

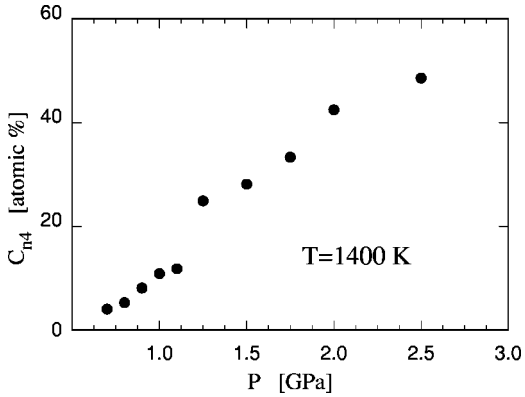

FIG. 11. Concentration of fourfold coordinated atoms as a function of P at $T=1400$ K.

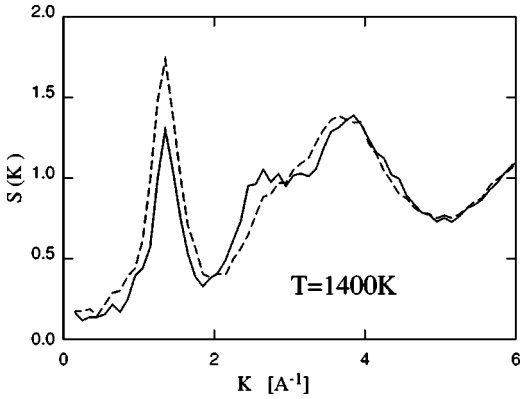

FIG. 13. Structure factor from a constrained simulation in which atomic coordination is limited to $n_c=2$ and $n_c=3$. Full line: polymeric sample at (2 GPa, 1400 K); dashed line: molecular fluid at (0.7 GPa, 1400 K).

K), but the concentration of fourfold coordinated atoms grows monotonically with increasing P, with an anomaly close to polymerization (Fig. 11). The population of fivefold coordinated atoms remains small ($\sim 0.3\%$ at $P=2$ GPa), and that of sixfold coordinated atoms is negligible. These results imply that polymerization does not lead to anything resembling a sc lattice, even if bending angles change from tetrahedral to cubic. Pressure also stabilizes undercoordinated atoms, but the population of twofold coordinated atoms never exceeds 2.6% for ($\leqslant 2.5$ GPa, 1400 K). The pressure evolution of the coordination number and of the local symmetry are determined implicitly by the values of δE_i^f and δE_i^b, and depends also on the form of the $F^j(\cos\theta)$ functions. These have been chosen to rule out any regular crystal phase of coordination $n_c>3$ at low T (and high density).

The P dependence of the local coordination is given by the probability distribution for bending angles $P(\theta)$ (Fig. 12).[33] At (0.8 GPa, 1400 K), $P(\theta)$ shows a high and narrow peak at 60° (the bond angle in P_4 tetrahedra), with a secondary peak from 85° to 110°. In the polymer phase at (2 GPa, 1400 K) the weight of the 60° peak decreases by a factor of 6, the peak around 90° becomes the most pronounced, and a new peak develops at 180°. These results are determined implicitly by the choice of the bending contribution to $U_b[\mathbf{R}_1,\ldots,\mathbf{R}_N]$, particularly its dependence on the coordination number. The results suggest that the changes of $g(r)$ and $S(K)$ across polymerization are affected significantly by the change in local symmetry from tetrahedral to sc. This is confirmed by a sequence of constrained simulations in which atomic coordination is restricted to 2 and 3, with the bending energy function $F^j(\cos\theta)$ fixed at the tetrahedral form. These simulations show that the constrained model polymerizes, and the polymerization pressure (between 1.25 and 1.5 GPa) is similar to the P_{polym} of the full model. The structure factor computed with the restricted model, however, differs from the experimental one (Fig. 13), and the average density at polymerization is $\sim 25\%$ lower than in the unrestricted simulation. The peak in $S(K)$ at 1.35 Å^{-1} survives well into the polymeric phase, confirming that it is not related directly to the concentration of P_4 units, but to the stability of the local tetrahedral bonding. These observations imply that the change in local coordination is not the driving force for polymerization, but the effect of polymerization under a sizable pressure.

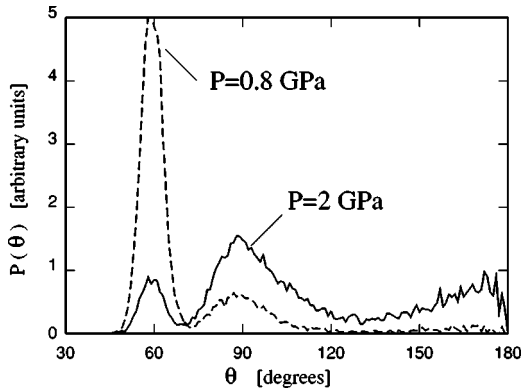

FIG. 12. Probability distribution for bending angles at (1 GPa, 1400 K) (dashed line) and at (2 GPa, 1400 K) (full line).

MC simulations provide no direct information on the real time dynamics, but the mobility μ of particles in phase space is related to the size and connectivity of the domain accessible to particles with energies of the order of K_BT. The simulations show that mobility is high in the dilute molecular fluid and low in the polymeric phase under pressure. A reduction of mobility with increasing P is expected, and standard statistical mechanics models[34] predict an exponential decrease of μ with increasing P (if μ is proportional to the diffusion coefficient D). This behavior is seen at low P (Fig. 14), but a sharp drop in $\mu(P)$ is apparent in the pressure range where polymerization occurs. The transition region is followed by a plateau at higher P. As apparent from Fig. 14, the mobility μ at $P\gg P_{polym}$ exceeds the values obtained by extrapolating the low-P data. The sudden decrease of mobility on polymerization can easily be rationalized, but the origin of the residual mobility at high P is less obvious. Most of the atoms belong to very large aggregates that do not diffuse, and the few small aggregates are surrounded by the dominant clusters. An important hint is provided by the results of a simulation at (1.75 GPa, 1400 K) starting from a well equilibrated polymeric sample, and continued at fixed configuration of covalent bonds. Freezing the bond dynamics decreases mobility by several orders of magnitude, showing

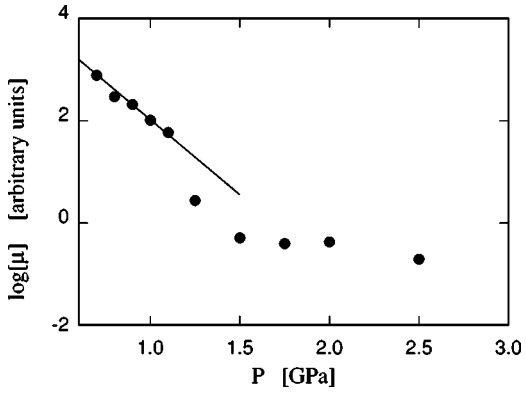

FIG. 14. Pressure dependence of the atomic mobilities computed by MC at $T=1400$ K.

that the residual diffusion is due to bond breaking, bond forming, and bond interchange processes. Diffusion in the polymeric phase is small, but might enhance the entropy of large aggregates and contribute to their stability at high P and T.

The reversibility of the transition has been demonstrated by decreasing P discontinuously from 2 GPa to 0.8 GPa (at $T=1400$ K) and monitoring the changes in thermodynamic properties. To avoid nucleating a low density phase within a high density connected system, simulations have been started from a sample with a large cluster but still undergoing polymerization (the cluster contained 60% of the total mass, compared with $>99\%$ in well equilibrated samples at 2 GPa). Figure 15 shows that the pressure drop is followed by a rapid decrease of the size $N_{\max}$ of the largest cluster and a slow recovery of the P_4 population. This suggests that the size of large clusters may change rapidly by adding or deleting a few bonds joining pivotal atoms belonging to distinct subaggregates. The concentration of a specific size (such as P_4) is the net effect of several competing reactions, resulting in slow relaxation.

The observation of depolymerization in liquid P is surprising, since the process can take up to days in reality. However, some model parameters affecting the activation energy

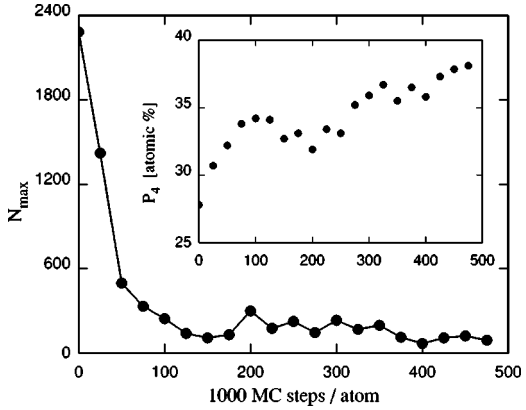

FIG. 15. Size of the largest cluster $N_{\max}$ and concentration (in atomic percent) of P_4 tetrahedra as a function of MC *time* following discontinuous pressure reduction from 2 to 0.7 GPa. The initial sample was not at equilibrium (see Sec. III).

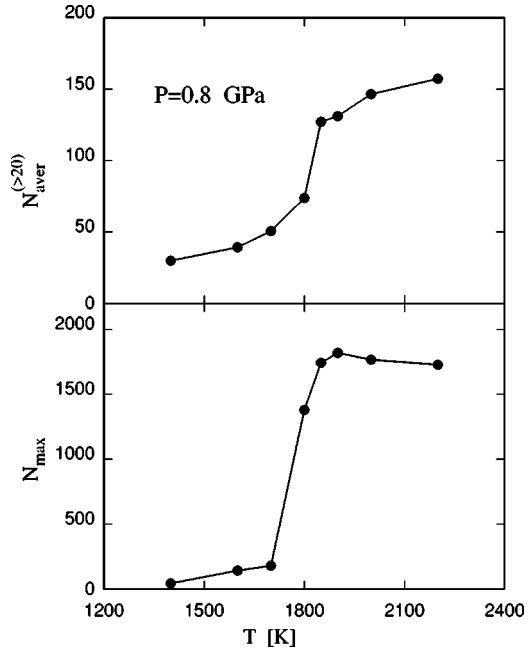

FIG. 16. Size $N_{\max}$ of the largest cluster after equilibration as a function of T at $P=0.8$ GPa; Average size $N_{aver}^{(>20)}$ of aggregates larger than 20 atoms. The system comprises 4000 atoms.

of bond interchanges (e.g., δE_i^f, δE_i^b, and the LJ parameters) have been chosen to enhance the bond kinetics, and the choice of MC method and the relative frequency of the different attempts affect greatly the relaxation kinetics and may avoid the kinetic bottlenecks of experiments.

The P-induced polymerization transition is shown clearly in the sequence of simulations performed at constant $P=0.8$ GPa, and T from 1400 K to 2600 K. The transition (at $T_{polym}\sim 1800-1850$ K) is evident in a plot of the size $N_{\max}$ of the largest cluster found in the simulated samples at the end of the equilibration stage (Fig. 16, lower panel). A sharp rise with increasing T is also observed in the same temperature range for the average size of clusters larger than 20 atoms ($N_{aver}^{(>20)}$). Unlike the results for P-induced polymerization, the near discontinuity in $N_{aver}^{(>20)}$ is much smaller than that of $N_{\max}$, since at (0.8 GPa, $\geqslant 1800$ K) a few large aggregates coexist with a sizable number of medium-size clusters ($N\sim 100$ atoms). Other differences between the transitions at constant P and at constant T are evident in the temperature dependence of the density, the local coordination, and the correlation functions (structure factor and radial distribution function).

Figure 17 shows that the density increases at constant P as T increases over a wide range, with no visible anomaly at the transition point. The density increase with increasing T is small, but surprising. An analysis of the structure, distances, and angular correlations shows that contraction is caused by the proliferation of medium size clusters, which is also seen in the monotonic increase of the average cluster size (Fig. 16). These aggregates are islands of relatively high density that increase with increasing T and raise the average density. The absence of a clear density anomaly at T_{polym} suggests that the sudden increase in the size of the largest cluster is a

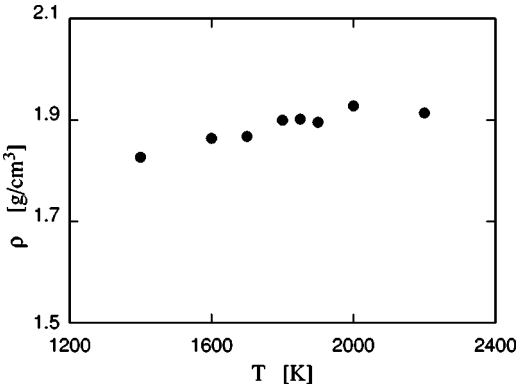

FIG. 17. Temperature dependence of the average density at $P=0.8$ GPa.

percolative process, due to the linking of clusters whose size and properties change continuously across the transition. The percolation threshold for a system of atoms on the continuum, involving a variable number of bonds is not known exactly. If we assume that percolation takes place when the population of relevant clusters reaches 30% of the total mass, we can identify the size of the aggregates giving rise to percolation as ~ 100 atoms.

Changes in the coordination and local symmetry are far less marked in T-induced polymerization than in P-induced polymerization. The concentration C_{n4} of fourfold coordinated atoms increases monotonically with increasing T, but the total number of fourfold coordinated atoms remains below $\sim 10\%$), and no anomaly is associated to the transition. The increase of C_{n4} with increasing T may be due to the fact that higher coordination dramatically enhances the number of distinct connected isomers that can be formed by a given number of atoms, thus increasing entropy.

Both $S(K)$ and $g(r)$ change much less at (0.8 GPa, 1850 K) than during P-induced polymerization. In particular, the changes in $S(K)$ (disappearance of the peak at 1.35 Å^{-1}, a split second peak at 2.8 Å^{-1} and 3.5 Å^{-1}) are much weaker or absent in the T-induced case. The peak at 1.35 Å^{-1} decreases and broadens slightly with increasing T, but it persists well into the polymer phase (Fig. 8). The asymmetry of the second peak at 2.5–4 Å^{-1} is enhanced slightly as T increases, but no splitting is seen up to ~ 2000 K. The radial distribution function above and below the polymerization temperature at $P=0.8$ shows that pair correlations are very similar in the molecular and polymeric phases at low P.

These results suggest that the polymer formed at (0.8 GPa, 1800 K) differs from that at ($\geqslant 1.25$ GPa, 1400 K). The former has a relatively low density (1.9 g/cm^3) and predominantly tetrahedral coordination, the latter has a higher density (2.3 g/cm^3), and the sc local symmetry dominates. Comparison with electronic structure computations for solid phases with comparable density and coordination suggests that the polymer at low P and high T is a semiconductor, with a metallic form at high P and moderate T. The temperature stabilization of the polymer phase will be reversed above a (higher) temperature T^*, because of the combined effect of translational and vibrational entropies. T^* will be affected by the thermal excitation of electrons with increasing T, which weakens covalent bonds. Our model does not contain this effect, and T^* is outside the temperature range studied and well above experimentally accessible temperatures.

V. DISCUSSION

An atomistic model developed to reproduce structural and energy properties of clusters and extended phases of phosphorus exhibits a liquid-liquid transition from a molecular to a polymer (gel) phase. This occurs with increasing P and/or T, and shows similarities to the transition revealed by recent x-ray diffraction experiments. Two paths in the (P-T) plane have been explored, the first covering 0.7–2.5 GPa at constant $T=1400$ K. Polymerization takes place between 1.1 and 1.25 GPa and is accompanied by a large change in the structure factor and an almost discontinuous increase in the average coordination number. The P dependence of the density is continuous over the entire range, with a rapid change of compressibility at the transition point. Most of the mass in the polymer forms a single large cluster, with small fragments breaking away and merging again with the cluster during the simulation.

The second path covers the range $T=1400-2200$ K. The sample polymerizes with increasing P at $T\sim 1850$ K, but the changes in $S(K)$ and the average coordination are less pronounced than in the P-driven transition. Polymerization arises from the aggregation of medium size clusters into a single large aggregate covering the entire sample. The high T means that the dominant clusters coexist with a significant population of medium-size aggregates.

The evolution of the computed structure factor along both paths follows closely the experimental trends, and the agreement could be improved even further by tuning the potential. The transition pressure at $T=1400$ K is overestimated by $\sim 10\%$, and the densities of the various phases are overestimated slightly. Despite these quantitative discrepancies, the description of the liquid-liquid transition agrees well with the experimental picture, and it can be used to address questions concerning the nature of the transformation.

The results confirm that the observed transition is polymerization, it has a close relation with the λ transition in S, and it is also driven by the entropy associated to the bond distribution. The identification of entropy as the driving force follows the observation that the transition can be obtained over a wide pressure range by changing T only. The liquid-liquid character is confirmed by the observation that the connected state is disordered at all P, and it is an equilibrium phase retaining a small but nonvanishing atomic mobility.

Polymerization at $T\sim 1400$ K and high P is accompanied by a rapid change in the local bonding geometry from tetrahedral to sc. Comparison of experimental and computational[12,25,35] results for phases of similar geometry and density suggests that the polymer phase is metallic. No similar change in the local bonding is observed upon polymerization at high T and low P, suggesting that the phase remains semiconducting. This implies that a semiconductor to metal transition also takes place in the polymer phase, possibly with a molecular-semiconductor polymer-metal polymer triple point at intermediate P and T. The model does not incorporate the electronic structure explicitly and

cannot locate this transition, but the results provide an impetus for further DF studies.

Other lines for future research are clear: First, the results suggest that the high T, low P polymerization is a percolative (continuous) transition, and the transformation appears to be continuous at higher P. A precise assessment of the transition order by computer simulation requires a finite-size scaling approach,[36] which is a formidable challenge for a model of this complexity. The present calculations, for example, took several single-CPU years on relatively fast processors. An alternative approach could be provided by the analysis of a Ginzburg-Landau free energy functional, possibly parameterized by the simulation results.

At low P and T, connected phases of phosphorus (black, red) are favored by potential energy over the molecular counterpart. At high T, the stability of connected phases is enhanced by the entropy of the covalent bond distribution. Here we note a possible difference between P and S. Potential energy favors the molecular phase in S, while favoring the connected phase of P. The entropy advantage of connected structures is more relevant in P, where the higher coordination increases the number of distinct configurations. It is then surprising that the stability range of molecular P is much wider than that of S. This may be resolved by noting that the free energy term competing with the bond distribution entropy is translational entropy, which is density dependent. The large volume increase upon melting favors the molecular phase, and this persists at low P up to high T. With increasing P, however, the low density of the molecular phase becomes a disadvantage, limiting the stability range of the molecular liquid.

Such questions would benefit from a systematic analysis of thermodynamic properties of liquid and amorphous phases, for which our model and simulations (together with DF computations) could provide input. Ours is not a definitive model for phosphorus, but it provides a flexible tool to establish relationships between features in the potential energy surface and its phase behavior.

ACKNOWLEDGMENTS

The simulations were performed in the FZ Jülich on Athlon, Xeon, and Compaq XP1000 computers provided in part by the Bundesministerium für Bildung und Wissenschaft, Bonn, within the MaTech-Kompetenzzentrum ''Werkstoffmodellierung'' (Grant No. 03N6015). The DF calculations were performed on a Cray SV1 computer in the FZ Jülich using time granted by FZ Jülich and the John von Neumann Institute for Computing (NIC).

[1] Y. Katayama, T. Mizutani, W. Utsumi *et al.*, Nature (London) **403**, 170 (2000).
[2] G. Monaco, S. Falconi, W. A. Crichton, and M. Mezouar, Phys. Rev. Lett. **90**, 255701 (2003).
[3] J. Donohue, *The Structures of the Elements* (Wiley, New York, 1974), p. 289.
[4] N. N. Greenwood and A. Earnshaw, *Chemistry of the Elements* (Pergamon, Oxford, 1984).
[5] R. W. G. Wyckoff, *Crystal Structures*, 2nd ed. (Wiley, New York, 1967), Vol. 1.
[6] J. H. Clarke, J. C. Dore, J. R. Granada, J. Reed, and G. Walford, Mol. Phys. **42**, 861 (1981); J. R. Granada and J. C. Dore, *ibid.* **46**, 757 (1982).
[7] J. C. Jamieson, Science **139**, 129 (1963); T. Kikegawa and H. Iwasaki, Acta Crystallogr., Sect. B: Struct. Sci. **39**, 158 (1983).
[8] J. Wittig and B. T. Matthias, Science **160**, 94 (1968); M. Okajima, S. Endo, Y. Akahama, and S. Narita, Jpn. J. Appl. Phys., Part 1 **23**, 15 (1984).
[9] D. R. Peck, in *Mellor's Comprehensive Treatise on Inorganic and Theoretical Chemistry* (Longman, London, 1971), Vol. 8, Suppl. 3, pp. 149–227.
[10] D. Hohl and R. O. Jones, Phys. Rev. B **50**, 17047 (1994).
[11] T. Morishita, Phys. Rev. Lett. **87**, 105701 (2001); Phys. Rev. B **66**, 054204 (2002).
[12] Y. Senda, F. Shimojo, and K. Hoshino, J. Phys.: Condens. Matter **14**, 3715 (2002).
[13] V. V. Brazhkin and A. G. Lyapin, J. Phys.: Condens. Matter **15**, 6059 (2003).
[14] Y. Katayama and K. Tsuji, J. Phys.: Condens. Matter **15**, 6085 (2003).
[15] R. O. Jones and P. Ballone, J. Chem. Phys. **118**, 9257 (2003).
[16] P. Ballone and R. O. Jones, J. Chem. Phys. **119**, 8704 (2003).
[17] R. Steudel, R. Strauss, and L. Koch, Angew. Chem. **97**, 58 (1985); B. Eckert and R. Steudel, Top. Curr. Chem. **231**, 31 (2003).
[18] L. Pauling and M. Simonetta, J. Chem. Phys. **20**, 29 (1951).
[19] P. Ballone and R. O. Jones (unpublished).
[20] R. O. Jones and D. Hohl, J. Chem. Phys. **92**, 6710 (1990); R. O. Jones and G. Seifert, *ibid.* **96**, 7564 (1992); Local density approximation to the exchange-correlation energy.
[21] P. Ballone and R. O. Jones, J. Chem. Phys. **100**, 4941 (1994). The exchange energy functional was from A. D. Becke, Phys. Rev. A **38**, 3098 (1988); The correlation functional was from J. P. Perdew, Phys. Rev. B **33**, 8822 (1986); **34**, 7406(E) (1986).
[22] DGAUSS program (UniChem package), Oxford Molecular (double zeta basis with polarization functions DZVP, auxiliary basis A1). The exchange-correlation energy used the gradient-corrected approximation PW91 [J. P. Perdew *et al.*, Phys. Rev. B **46**, 6671 (1992).]
[23] H. Iwasati and T. Kikegawa, Acta Crystallogr., Sect. B: Struct. Sci. **53**, 353 (1997).
[24] Y. Akahama, H. Kawamura, S. Carlsen *et al.*, Phys. Rev. B **61**, 3139 (2000).
[25] K. J. Chang and M. L. Cohen, Phys. Rev. B **33**, 7371 (1986).
[26] H. Östmark, S. Wallin, N. Hore, and O. Launila, J. Chem. Phys. **119**, 5918 (2003).
[27] The LJ potential is continued by a third order polynomial between 3σ and 3.2σ, and is zero for $r>3.2\sigma$. The coefficients of the polynomial are chosen so that the potential and its first derivative are continuous everywhere.
[28] Modern DF methods should provide a unified description of the moderate T portions of the phase diagram, although the computational cost still prevents extensive simulations.
[29] Updated value. See Ref. 22.
[30] V. V. Brazhkin, R. N. Voloshin, S. V. Popova, and A. G. Lyapin, *New kinds of Phase Transitions: Transformations in Disordered Substances*, edited by V. V. Brazhkin, S. V. Buldyrev, V. N. Ryzhov, and H. E. Stanley (Kluwer, Dordrecht, 2002).
[31] The decomposition of P_4 into $2P_2$ is highly endothermic, occurring only at very high T and low density.
[32] M. Häser, U. Schneider, and R. Ahlrichs, J. Am. Chem. Soc. **114**, 9551 (1992).
[33] The probability distribution function $P(\theta)$ is normalized so that $\int_0^\pi P(\theta)\sin\theta d\theta=1$. Averages over bending angles of a function $f(\theta)$ are defined by $\langle f\rangle=\int_0^\pi f(\theta)P(\theta)\sin\theta d\theta$
[34] W. Götze and A. Sjölander, Rep. Prog. Phys. **55**, 241 (1992).
[35] K. J. Chang and M. L. Cohen, Phys. Rev. B **33**, 6177 (1986).
[36] D. P. Landau and K. Binder, *A Guide to Monte Carlo Simulations in Statistical Physics*, (Cambridge University Press, Cambridge, UK, 2000).